The Time-varying Networks of the Wrist Extension in Post-stroke Hemiplegic Patients

Fali Li
University of Electronic Science and Technology of China https://orcid.org/0000-0002-2450-4591
Lin Jiang
University of Electronic Science and Technology of China
Yuqin Li
University of Electronic Science and Technology of China
Dongfeng Huang
Sun Yat-Sen University
Yuanling Jiang
University of Electronic Science and Technology of China
Yueheng Peng
University of Electronic Science and Technology of China
Xiabing Zhang
University of Electronic Science and Technology of China
Dezhong Yao
University of Electronic Science and Technology of China
Peng Xu
University of Electronic Science and Technology of China
Hai Li (lihai2018@smu.edu.cn)
Sourthern Medical University

Research

Keywords: Stroke, motor dysfunction, time-varying networks, wrist extension, ipsilateral compensatory

Posted Date: October 29th, 2020

DOI: https://doi.org/10.21203/rs.3.rs-97653/v1

The time-varying networks of the wrist extension in post-stroke hemiplegic patients

Fali Li[1,2#], PhD; Lin Jiang[1,2#], BD; Yuqin Li[1,2], BD; Dongfeng Huang, MD; Yuanling Jiang[1,2], MD; Yueheng Peng[1,2], MD; Xiabing Zhang[1,2], MD; Dezhong Yao[1,2], PhD; Peng Xu[1,2]*, PhD; Hai Li[4]*, MD, PhD

[#]The first two authors contributed equally to this work.

*Correspondence:

Prof. Peng Xu (xupeng@uestc.edu.cn) or Dr. Hai Li (lihai2018@smu.edu.cn)

Abstract

Background: Hemiplegia is a common dysfunction caused by a stroke and leads to movement disability. Although the movement-related oscillation, the lateralization of the movement-related potential, and the event-related desynchronization have been investigated, the dynamic network modalities related to the movements in post-stroke hemiplegic patients are still left unveiled.

Methods: In our present study, we designed the motor execution task of the wrist extension, collected the movement-related electroencephalograms, and adopted the

adaptive directed transfer function to investigate the dynamic motor networks in post-stroke hemiplegic patients. The corresponding time-varying networks of the wrist extension in post-stroke hemiplegic patients were constructed and then statistically explored.

Results: The results demonstrated that the effective connectivity between the stroked motor area and other areas decreased. In contrast, connectivity between non-stroked motor area and other areas was enhanced, especially the frontal and parietal-occipital lobes, to compensate for the dysfunction of the motor behaviors of the stroked patients.

Conclusions: These findings help us better understand the time-varying networks underlying the implementation of the motor behaviors of the patients with post-stroke hemiplegia and might provide a reliable biomarker to predict their future rehabilitation.

***Keywords*:** Stroke, motor dysfunction, time-varying networks, wrist extension, ipsilateral compensatory

Background

Stroke, also known as cerebrovascular accident, is a disease of brain damage caused by the sudden burst of cerebral blood vessels or the block of blood vessels, including hemorrhagic and ischemic stroke. Stroke has high morbidity, disability, and mortality

rates, and 40% of stroke survivors still live with various disabilities. After a stroke, multiple functions are seriously impaired, and the most common one is post-stroke contralateral limb hemiplegia [1]. Such a wrist or upper limb dysfunction usually lasts a lifetime. Wrist extension is an essential part of hand touching object movement. Severe wrist paralysis is still a considerable challenge in clinical practice, which impacts the patients with their activities of daily living functions and the quality of life.

Symptoms of post-stroke limb disorders depend on the location of the brain in the left or right hemisphere. The stroke of the dominant left hemisphere may behave communication disorder and the paralysis of the right hand and foot. While lesions in the right hemisphere might lead to the impairment of perception (visual impairment) and the paralysis of the left hand and foot. Compared with the right hemisphere stroke, the dysfunction caused by the left hemisphere stroke is usually easier to be identified and diagnosed on time. In this study, we mainly took middle-aged and older people as the subjects to investigate the differences in time-varying network architectures between patients with unilateral stroke and the control group during wrist extension.

Currently, the studies focusing on the brain network mechanism of the post-stroke motor dysfunction have depended mainly on functional magnetic resonance imaging (fMRI). The implementations of the motor behaviors in healthy controls (HCs) are usually achieved by simultaneous activation of multiple motor-related brain regions, including supplementary motor area (SMA), sensorimotor area, primary motor area,

prefrontal lobe, and bilateral dorsal anterior motor area, etc. [2, 3]. The changes in the ipsilateral motor cortex of the stroked hemisphere are usually more complicated for post-stroke hemiplegic patients. For example, after analyzing the changes in the functional connectivity of bilateral primary motor areas, Li et al. found the decreased functional connectivity in stroke patients [4]. Zhao et al. used independent component analysis to explore related functional networks of stroked patients and found connectivity within and between motor-related networks were both abnormal, especially the decline in the dorsal attention network and the overcompensation of the executive control network [5]. Moreover, the increased activation of frontal and parietal regions and motor areas in stroke patients has also been found to be associated with the motor behaviors, as well as those non-motor areas such as the occipital lobe [6-8].

Concerning the electrophysiological characteristic, the brain activity in the sensorimotor rhythm of the 8 - 30 Hz has been widely studied, and the electroencephalogram (EEG) is thus usually used to investigate the sensorimotor rhythm related to the motor behaviors, as well as its application in stroke [9]. However, recent studies have mainly concentrated on EEG oscillation related to the movement and the lateralization of the movement-related potential and the event-related desynchronization for stroke patients and HCs [10, 11], but less attention has been put on the dynamic network modalities related to the movements concerning the post-stroke hemiplegic patients.

The brain is a complex network, and the completion of motor execution is completed by the interaction of multiple brain regions. Stroke patients also include multiple motor and non-motor related brain regions to achieve limb movement [12]. The investigation of the dynamic networks during motor execution helps understand the motor dysfunction in stroke patients. Considering the EEG has a relatively high time resolution, we can further explore the dynamic interactions among different brain regions in milliseconds. The adaptive directed transfer function (ADTF) [13] has been widely used to calculate the effective connectivity in milliseconds. It facilitates the construction of the time-varying networks on each time point, which thus provides the opportunity to estimate the directed flows among concerned brain regions and to capture the dynamic transition related to the movement effectively. For example, based on the ATDF, Li et al. have demonstrated the distinct information processing stages related to the P300 [14] and the motor imagery [15], as well.

To better investigate the differences in dynamic network architectures between the stroke patients and HCs during the motor execution, in our present study, we applied the ADTF in three subject groups, i.e., HCs, post-stroke hemiplegic of the left arm (PL), and post-stroke hemiplegic of the right arm (PR), to construct their time-varying networks related to the wrist extension. Thereafter, the potential differences concerning the three groups were further investigated from the perspective of the dynamic network topology and property to better understand the motor dysfunction that occurred in post-stroke hemiplegic patients.

Methods

Participants

The study protocol was approved by the ethics committee of the First Affiliated Hospital of Sun Yat-sen University. Twenty-seven participants were recruited in the present study, which included 9 PL patients (7 males, age 56.1 ± 10.7 years), 7 PR patients (6 males, age 55.7 ± 8.8 years), and 11 HCs (5 males, age 52.8 ± 7.6 years). All participants were informed of the study protocol, along with the signed informed consent forms. Meanwhile, all subjects were self-recognized as right-handed and confirmed by the Edinburgh Handedness Inventory.

Experimental procedure

E-prime (Psychology Software Tools, Inc, USA) was used to present the visual directions or cues in the study. The paradigm of the Instruction Response Movement (IRM) was adopted to present a solid arrow picture pointing either to the left or the right (regarded as "GO" signals in this study). Accordingly, the subjects were requested to perform left or right wrist extension. In each IRM trial (Fig. 1), a white cross in the center of a black screen serves as an attention point, which lasted for a duration ranging from 1000 ms to 2000 ms randomly. The left or right "GO" signal then appeared randomly at the screen for a duration of 3000 ms, and the subject started to perform the required motion once for each trial when they noticed the

presence of the "GO" signal, which included 40 trials for each side movement. After finishing the movement, subjects rested their arms on the table, and a black screen lasting for 2000 ms was presented for a short rest. Before starting to record the EEG, subjects would also practice the required movement for 1 min to 2 mins to get familiar with our experiments.

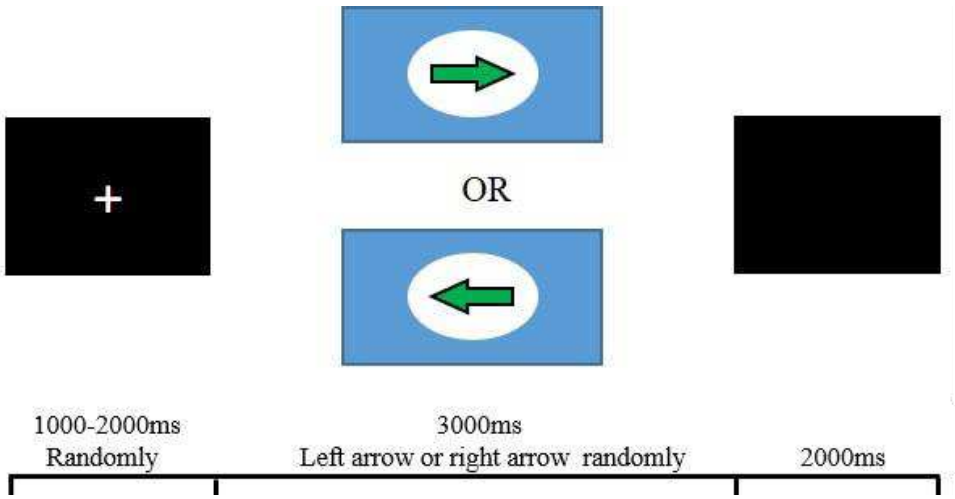

Fig. 1. The experimental procedures and the timeline of a task trial.

EEG recording

All of the experiments were conducted in a shielded room, which provided the insulation from electromagnetic signals and background noise distractions. A BrainAmp 32-channel amplifier from Brain Products (Munich, Germany) was used to record EEG. All of the 32 Ag/AgCl electrodes were placed according to the 10–20 international system. The online digital sampling rate is 1000 Hz, and electrodes FCz and AFz were used as the reference and ground, respectively. Electrooculogram (EOG) was measured by two extra electrodes, one above the middle point of the right brow to

record the EOG vertically, and the other was placed 2 cm aside from the outer corner of the right eye to record the EOG horizontally. To guarantee reliable data quality, throughout the experiment, the impedance for all electrodes was kept below 5 kΩ.

EEG data analysis

In this study, the recorded EEG was first pre-processed to acquire the artifact-free trials and then used to construct the corresponding time-varying effective connectivity networks, which was carried out using MATLAB v2014a (The MathWorks Inc., Natick, MA). The details were further depicted in the following sections.

EEG data pre-processing

The EEG was first band-pass filtered with a frequency range of [1, 30] Hz, and based on the independent component analysis (ICA), the ocular was then corrected semi-automatically. Thereafter, the EEG was re-referenced to a neutral reference of the Reference Electrode Standardization Technique (REST) [16, 17]. Meanwhile, multiple procedures consisting of [-1, 000 2, 000] ms range (0 ms corresponds to the stimulus onsets) data segmentation, [-1, 000 -800] ms baseline correction, and artifact removal (using a threshold of ±75 μV) were also included, and the researchers further visually inspected the remaining trials to exclude those still contain residual artifacts. Afterwards, 24 canonical electrodes (i.e., Fp1/2, Fz/3/4/7/8, FC1/2, T7/8, Cz/3/4, CP1/2, Pz/3/4/7/8, and Oz/1/2) were used in the following analysis.

164

165 Power spectral density

166 For each subject, the power spectral density (PSD) of each electrode was first
167 estimated using the pWelch at α (8 - 13) and β (13 - 30 Hz). When exploring the
168 group differences, the PSD of the PL, PR, and HC groups were statistically compared
169 by using the non-parametric Wilcoxon rank-sum test, whose *p*-values were then
170 multiply corrected by the false discovery rate (FDR) under a significance level of 0.05
171 ($p < 0.05$).

172

173 Time-varying network

174 To unveil the dynamic network pattern underlying the required motion, the ADTF [13]
175 was used to construct corresponding time-varying networks of this motion, which
176 were further statistically compared to identify the group-wise differences of dynamic
177 network patterns between PL, PR, and HC groups. In specific, for each subject, the
178 remaining artifact-free trials were down-sampled to 100 Hz, resulting in the 10 ms
179 interval between two neighboring sample points, and based on the trial-by-trial ADTF,
180 the time-varying networks were then constructed.

181

182 *1) Time-varying Multivariate Adaptive Autoregressive (tv-MVAAR) Model*

183 For each trial time series, the tv-MVAAR model was defined and then calculated with
184 the following equation,

$$X(t) = \sum_{i=1}^{p} A(i,t)X(t-i) + E(t) \quad (1)$$

where $X(t)$ denotes the artifact-free EEG vector at time point t, $A(i,t)$ denotes the matrix of the tv-MVAAR model coefficients estimated by the Kalman filter algorithm [18], $E(t)$ is the multivariate independent white noise, and p is the optimal model order automatically determined by the Akaike Information Criterion [19],

$$AIC(P) = \ln[\det(\sum)] + 2M^2P / N \quad (2)$$

where M is the number of EEG channels, P is the estimated tv-MVAAR model order, N is the time point, and Σ is the covariance matrix. The observation and state equations were then solved by the recursive least squares algorithm with the forgetting factor [20].

2) Adaptive Directed Transfer Function

After acquiring the time-varying tv-MVAAR model coefficient $A(i,t)$, its transformation in the frequency domain, $H(f,t)$, would also be obtained, and the H_{ij} element of $H(f,t)$ represents the directed information flow from the j-th to the i-th element for each time point t at frequency f. And accordingly, Eq. (1) is then further transfer to the frequency domain as

$$A(f,t)X(f,t) = E(f,t) \quad (3)$$

$$X(f,t) = A^{-1}(f,t)E(f,t) = H(f,t)E(f,t) \quad (4)$$

where $A(f,t) = \sum_{k=0}^{p} A_k e^{-j2\pi f \Delta t k}$ with A_k being the matrix of the tv-MVAAR model

coefficients, and $X(f,t)$ and $E(f,t)$ are the transformations of $X(t)$ and $E(t)$ in the frequency domain, respectively.

The normalized ADTF, which describes the directed information flow from the j-th node to the i-th node at frequency f and time t, is defined with a range of [0, 1] as,

$$\gamma_{ij}^2(f,t) = \frac{\left|H_{ij}(f,t)\right|^2}{\sum_{m=1}^{n}\left|H_{im}(f,t)\right|^2} \tag{5}$$

And the integrated ADTF is finally defined as the average of the normalized ADTF over the interested band $[f_1, f_2]$ at time t, which was defined in a frequency range of [8, 30] Hz in our present study.

$$\Theta_{ij}^2(t) = \frac{\sum_{k=f_1}^{f_2}\gamma_{ij}^2(k,t)}{f_2 - f_1} \tag{6}$$

After acquiring the ADTF adjacency matrix for each artifact-free motion trial, the trial-average of the ADTF matrices was obtained to define the final time-varying networks for each subject. When exploring the group-wise differences, the time-varying weighted networks of the PL, PR, and HC groups were first binarily thresholded into the time-varying binary networks with a connectivity cost of 5% to illustrate the intrinsic network architectures and were also statistically compared by using the non-parametric Wilcoxon rank-sum test whose p-values were also multiply corrected by FDR ($p < 0.05$).

Network properties

Based on graph theory, the time-varying global efficiency (*GE*) was calculated by using the brain connectivity toolbox (BCT, http://www.nitrc.org/projects/bct/) [21], which were still based on the constructed time-varying weighted networks. The *GE* describes the ability of the time-varying networks to process information.

$$GE = \frac{1}{n}\sum_{i\in\Psi}\frac{\sum_{j\in\Psi, j\neq i}\left(\sum_{a_{ij}\in g_{i\to j}} a_{ij}\right)^{-1}}{n-1} \tag{7}$$

where n denotes the node number, Ψ denotes the set of all network nodes, a_{ij} denotes the estimated ADTF connectivity strength and $g_{i\to j}$ denotes the weighted directed shortest path from nodes i-th to j-th.

Results

PSD

The PSD of the three groups in 8 - 30 Hz was obtained, and as illustrated in Fig. 2, the electrodes whose statistical p-values pasted the test were marked out. The scalp topographies exhibiting stronger PSD for the PL subjects were found to locate at the parietal and occipital areas compared to HC subjects when executing the left-hand wrist movement (Fig. 2a, $p < 0.05$), while no differences were revealed between PR and HC groups when performing the right-hand wrist extension (Fig. 2b, $p > 0.05$).

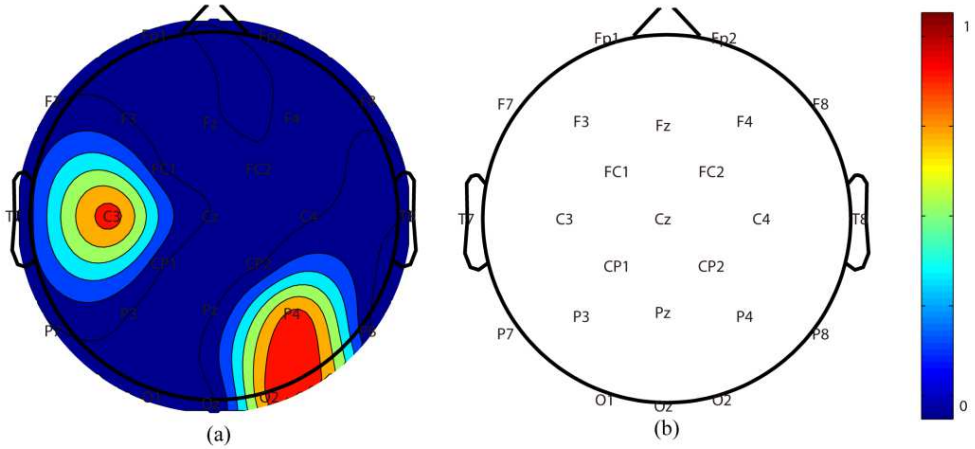

241

242 **Fig. 2.** Scalp PSD topographies in 8 - 30 Hz. (a) Between PL and HC groups and (b)
243 Between PR and HC groups. The regions printed with deep red color denote the PSD
244 of the PL/PR group is significantly greater than the HC group, and the blue denotes
245 the opposite.

246

247 Differential time-varying network patterns

248 To investigate the time-varying patterns of brain networks in HC, PL, and PR groups
249 during wrist extension, the effective connectivity at each time point was averaged
250 across subjects and then sparsed with 5% sparseness (i.e., the connection edge with
251 the strongest weight remaining 5%) to display the transient network topology. As
252 displayed in Fig. 3, for the HC subjects (Fig. 3a), the electrodes C3 or C4 served as
253 the crucial hub to control the right or left-hand wrist extension at first, which then
254 transferred to the joint control from bilateral C3 and C4 electrodes. However, for the
255 PL subjects (Fig. 3b), the motor area of the stroked hemisphere (i.e., right hemisphere)
256 showed seldom connectivity when starting to perform the left-hand wrist extension,
257 but the contralateral F3 and C3 electrodes (i.e., at the left hemisphere) extended to the

occipital lobe showed the stronger connectivity architectures; while for the PR subjects (Fig. 3c), the crucial hubs were found to be located at the contralateral C4 and P4 and ipsilateral P3, when performing the right-hand wrist extension.

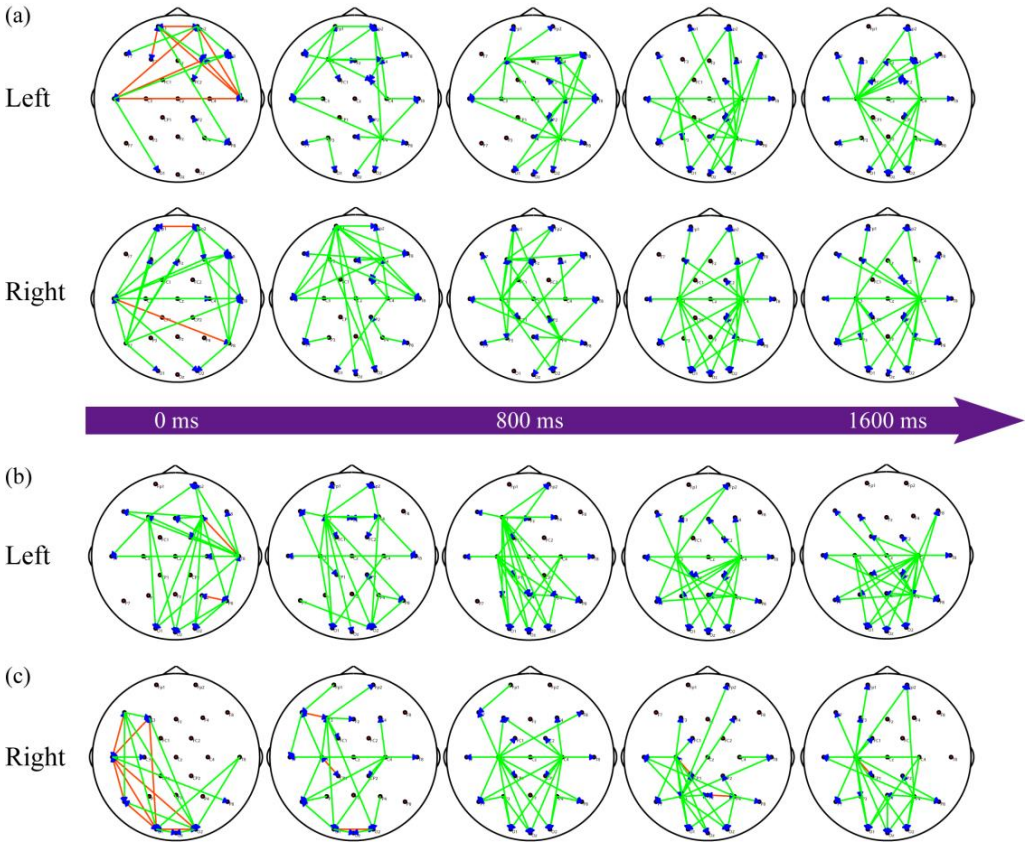

Fig. 3. Time-varying information flow when achieving the wrist extension. (a) HC subjects, (b) PL subjects, and (c) PR subjects. In each subfigure, the solid green lines indicate the directed information flows, the arrows indicate the directions of information flows, and the solid red lines denote bidirectional information flows.

To further explore the differential dynamic network patterns between post-stroke hemiplegic patients and healthy people during motor execution, Fig. 4 further displays the corresponding statistical network topologies. When comparing the PL and HC

subjects (Fig. 4a), the electrodes having stronger information flow in the PL group transferred from the occipital lobe (e.g., Oz) to the left frontal lobe (e.g., F7); however, for the PS subjects (Fig. 4b), this transmission occurred from occipital lobe (e.g., Oz) and left frontal lobe (e.g., F7) to the right temporal lobe (e.g., T6).

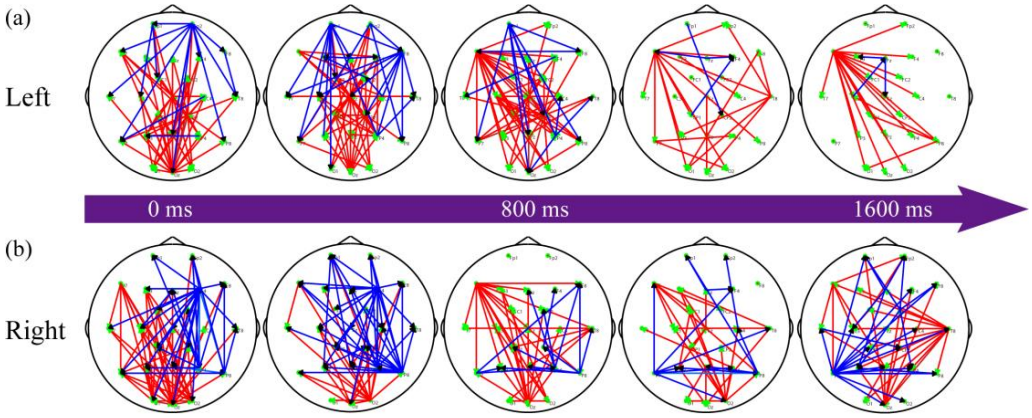

Fig. 4. Differential time-varying network topologies between the pairwise groups. (a) PL versus HC groups and (b) PR versus HC groups. In each subfigure, the red and blue solid lines indicate significantly stronger and weaker directed information flows of the PL/PR group than the HC group, respectively.

Dynamics of the time-varying *GE*

The time-varying *GE* of all subjects in PL, PR, and HC groups at different time points were averaged, as illustrated in Fig. 5(a), during the wrist extension, the *GE* increased along with the motion. And when quantitatively measuring the potential differences, Fig. 5(b) further illustrated that only when performing left-hand wrist extension, the *GE* of the PL group was greater than that of the HC group ($p < 0.05$).

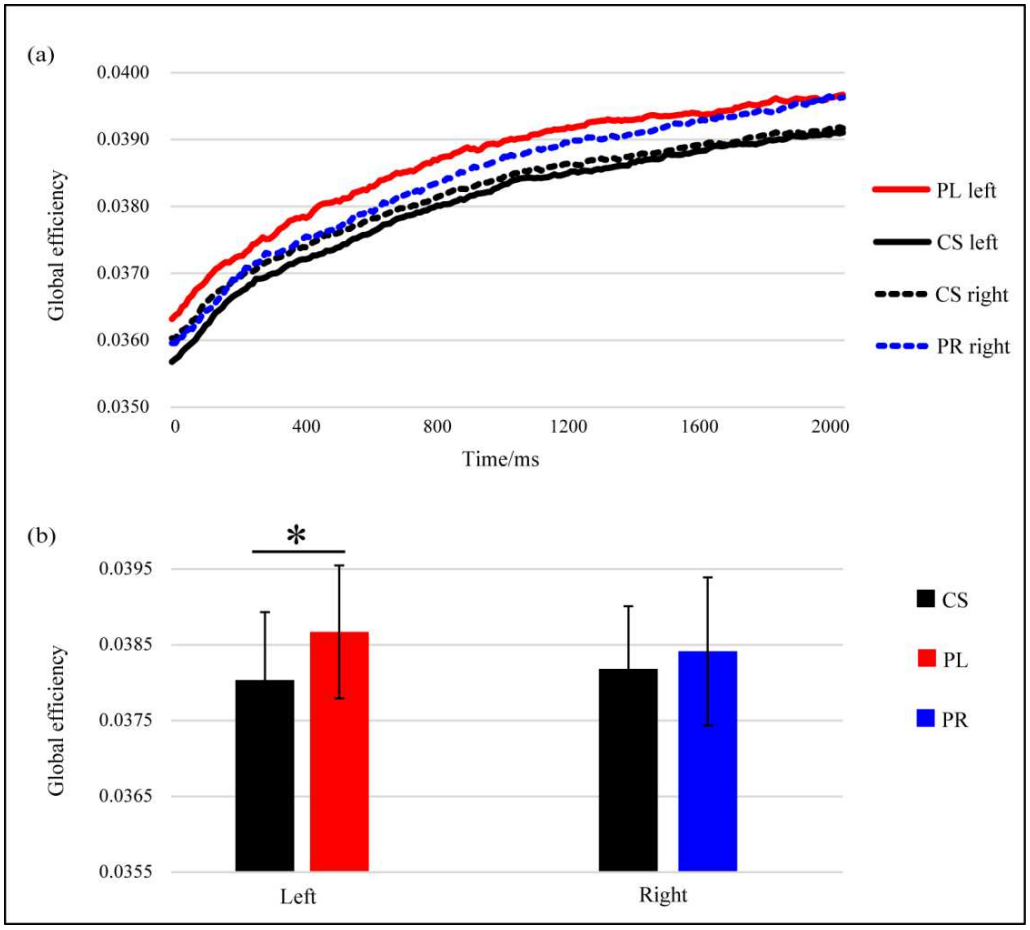

286

287 **Fig. 5.** The time-varying *GE* of the three groups. (a) Dynamics of the *GE* and (b)

288 Statistics of the average *GE*.

289

290 **Discussion**

291 Stroke is one of the most important diseases that threaten our lives and further leads to

292 motor impairments in stroke survivors. Compared with healthy people, the interaction

293 among different brain regions is more complicated in post-stroke patients when

294 accomplishing the movements. Hence, in the current study, we proposed to adopt the

295 ADTF to investigate the dynamic network architectures of movement-related activity

296 during the wrist extension in post-stroke hemiplegic patients and healthy people.

297 Before applying the ADTF, the different PSD topographies were first investigated,
298 as displayed in Fig. 2, although the stronger activities at the left primary motor areas
299 (e.g., C3) and right parietal and occipital lobes (e.g., P4 and O2) were found for the
300 PL group compared to the HC group, no differences were found for the PR group.
301 This result suggested that the contralateral brain areas corresponding to the stroked
302 hemisphere of PL patients were strongly activated than that of healthy people to
303 compensate for the damaged lateral brain areas. Unfortunately, the PSD failed to
304 uncover the detailed interactions among different brain areas that were related to the
305 wrist extension, which seemed to be more helpful for our understanding of the
306 post-stroke motion.

307 To explore the dynamic interaction in post-stroke hemiplegic patients (i.e., PL
308 and PR groups) and healthy people (i.e., HC group) across different brain regions,
309 time-varying network topologies of the left- and right-hand wrist extension were
310 calculated and then illustrated in Fig. 3. As displayed in Fig. 3(a), when the "GO"
311 signal appeared, the networks of earlier motor execution stage (i.e., networks of 0 ms
312 to 800 ms) for the HC subjects showed strong contralateral connectivity coupling
313 among right motor area concerning the left-hand wrist extension, while left motor
314 area showed significant stronger connectivity during right-hand movement, which
315 then switched to a bilateral connectivity architecture (i.e., networks of 800 ms to 1,
316 600 ms) with C3 or C4 as hub node. Previous studies have demonstrated that medial
317 frontal gyrus, parietal lobe, primary motor cortex, and SMA are highly involved

during motor execution and exhibit contralateral hemispherical responses corresponding to the moving hand [22, 23], and similar to the motor imagery, during the posterior of the required motion, this contralateral hub would be transferred to the bilateral hubs to accomplish this motion [15], which was consistent with our current findings.

However, since the stroke occurred in PL and PR subjects, as a result, the network patterns of PL and PR patients would be different from that of healthy people, and the site and severity of stroke will further affect the degree of neural plasticity related to the motor-related network architecture [11]. Specifically, investigating Fig. 3(b), when performing the left-hand movement (i.e., networks of 0 ms to 800 ms), stronger functional coupling existed between F3/C3 and parietal-occipital lobe, while seldom connectivity of the stroked right hemisphere was observed, which might account for the deficits in the left-hand wrist extension of the PL subjects. The frontal lobe is activated to be responsible for the control of body movements, and to compensate for the deficits brought by the stroked right hemisphere, the ipsilateral hemisphere then provides the functional compensation for the body movements [24, 25]. Thereafter, hub nodes transferred from F3 and C3 to bilateral motor areas (i.e., C3 and C4, networks of 800 ms to 1600 ms), which was similar to that of the HC subjects. While concerning the right-hand movement of the PR subjects, as displayed in Fig. 3(c), stronger flows (i.e., networks of 0 ms to 800 ms) directed from F3 were observed, as well as the bilateral parietal lobe at 1, 600 ms whose hubs were P3 and

P4, which might further clarify that besides the participation of the contralateral motor area of the stroked hemisphere, the other non-motor areas in the injured hemisphere that were responsible for the high-level cognition, such as motor planning and attention, may also be involved.

To further explore the impaired effective connectivity in PL and PR patients, Fig. 4 then illustrated the different patterns of time-varying networks between PL/PR and HC group during hand movement. The PL patients exhibited enhanced connectivity to frontal-parietal and motor areas starting from Oz compared with the HC group, which is bottom-up architecture (i.e., networks of 0 ms and 400 ms). The occipital lobe is responsible for visual information processing. After receiving the "GO" signal (i.e., 0 ms), the upper limb dyspraxia in stroke patients led to the delayed movement, the enhanced bottom-up connectivity might then intensify the motion intention of the required wrist extension [26], and during the later motion stage (i.e., from 800 ms to 1, 600 ms), the hub gradually transferred from Oz to F7 (Fig. 4a), and the top-down modulation starting from F7 to bilateral parietal-occipital lobe is significantly enhanced. As illustrated above, frontal and parietal regions play an irreplaceable role in motion planning and decision-making associated with motor regulation [27]. When planning the motion, the parietal lobe is regulated by the prefrontal lobe. That is, their cooperation helps complete the assigned tasks [28]. However, the stroke in PL patients destroyed the high-level regulatory involved in exercise execution, to compensate for the completion of the wrist execution, in our present study, the

enhanced connectivity in the contralateral frontal-occipital lobe of the stroked hemisphere was, therefore, observed for the PL subjects. Concerning the PR patients (Fig. 4b), the hubs transferred from the occipital lobe (e.g., Oz) and left frontal lobe (e.g., F7) to the right temporal lobe (e.g., T6), and although the stroke resulted in the dysfunction of the patients' motor network, more contralateral hemispheric and ipsilateral non-motor regions were included to compensate for the wrist extension [24, 25], and accordingly, the enhanced time-varying network architectures connecting related areas facilitated the stroked patients with their motion.

Moreover, *GE* is the average efficiency of the related brain network and is usually applied to estimate the potential for functional integration among brain areas. Besides the above network architecture, just as illustrated in Fig. 5, during the wrist extension, the time-varying *GE* of the HC, PL, and PR groups increased along with the execution. We speculated that it might be due to the plasticity changes between different brain regions after stroke, patients with post-stroke hemiplegic activated more other brain regions as compensation, and the increased interaction could dynamically compensate for the injured hemisphere to complete our required movement. And indeed, in our present study, when performing the left-hand wrist extension, the average *GE* of the PL group was significantly larger than that of the HC group (Fig. 5b).

Conclusions

In conclusion, by using the ADTF, we investigated the time-varying network patterns

of the PL, PR, HC groups when they were performing the required wrist extension. We found the obvious transition of the control hub from the contralateral to the bilateral hemisphere for the HC subjects. However, concerning the PL and PR patients, when performing the wrist extension, the effective connectivity between stroked motor area and others was weaker while that between non-stroked motor area and others was enhanced for the motor planning and regulation, especially the frontal and parietal-occipital lobes, to compensate for the dysfunction of the motor behaviors for the stroked patients. These findings help us better understand the network mechanism underlying the motor dysfunction of the patients with post-stroke hemiplegic and might also serve as a reliable biomarker applied to the future rehabilitation of stroke patients.

Abbreviations

HC: Healthy Controls; ADTF: Adaptive Directed Transfer Function; PL: Post-stroke hemiplegic of the Left arm; PR: Post-stroke hemiplegic of the Right arm; IRM: Instruction Response Movement; REST: Reference Electrode Standardization Technique; tv-MVAAR: time-varying Multivariate Adaptive Autoregressive; GE: Global Efficiency; SMA: supplementary motor area; EEG: electroencephalogram; EOG: Electrooculogram; ICA: independent component analysis; PSD: power spectral density; FDR: false discovery rate.

Authors' contributions

HL and DFH designed the experiment protocol. HL collected the data. FLL, LJ, YQL, and YLJ analyzed the data. Results were interpreted by FLL, LJ, YLJ, and YHP. The draft was written by FLL and LJ under supervision of YDZ and PX. HL and XBZ provided constructive suggestion for writing this draft. All authors read and approved the final manuscript.

Funding

This work was supported by the National Natural Science Foundation of China (#61961160705, #U19A2082, #61901077), the National Key Research and Development Plan of China (#2017YFB1002501), the Key Research and Development Program of Guangdong Province, China (#2018B030339001), the 5010 Planning Project of Sun Yat-sen University of China (Grant No. 2014001), and the Science and Technology Development Fund, Macau SAR (File no. 0045/2019/AFJ).

Availability of data and materials

The datasets used and/or analysed during the current study are available from the corresponding author on reasonable request.

Ethics approval and consent to participate

The study protocol was approved by the ethics committee of the First Affiliated

Hospital of Sun Yat-sen University. All participants were informed of the study protocol, along with the signed informed consent forms.

Consent for publication

All participating subjects signed informed consent for this study and subsequent publications, and all identifying features were removed.

Competing interests

The authors declare that they have no competing interests.

Author details

[1]The Clinical Hospital of Chengdu Brain Science Institute, MOE Key Lab for Neuroinformation, University of Electronic Science and Technology of China, Chengdu, 611731, China

[2]School of Life Science and Technology, Center for Information in BioMedicine, University of Electronic Science and Technology of China, Chengdu, 611731, China

[3]Department of Rehabilitation Medicine, The Seventh Affiliated Hospital, Sun Yat-sen University, Guangzhou, 510275, China

[4]Neurorehabilitation Laboratory, Department of Rehabilitation Medicine, Shenzhen Hospital, Southern Medical University, Shenzhen, 518100, China

References

1. Winstein, C.J., J. Stein, R. Arena, B. Bates, L.R. Cherney, S.C. Cramer, et al. Guidelines for Adult Stroke Rehabilitation and Recovery: A Guideline for Healthcare Professionals From the American Heart Association/American Stroke Association. Stroke. 2016;47(6):e98-e169.
2. Roland, P.E., B. Larsen, N.A. Lassen, and E. Skinhoj. Supplementary motor area and other cortical areas in organization of voluntary movements in man. J Neurophysiol. 1980;43(1):118-36.
3. Vry, M.S., D. Saur, M. Rijntjes, R. Umarova, P. Kellmeyer, S. Schnell, et al. Ventral and dorsal fiber systems for imagined and executed movement. Exp Brain Res. 2012;219(2):203-16.
4. Li, Y., D. Wang, H. Zhang, Y. Wang, P. Wu, H. Zhang, et al. Changes of Brain Connectivity in the Primary Motor Cortex After Subcortical Stroke: A Multimodal Magnetic Resonance Imaging Study. Medicine (Baltimore). 2016;95(6):e2579.
5. Zhao, Z., J. Wu, M. Fan, D. Yin, C. Tang, J. Gong, et al. Altered intra- and inter-network functional coupling of resting-state networks associated with motor dysfunction in stroke. Hum Brain Mapp. 2018;39(8):3388-97.
6. Ward, N.S., M.M. Brown, A.J. Thompson, and R.S. Frackowiak. Neural correlates of motor recovery after stroke: a longitudinal fMRI study. Brain. 2003;126(Pt 11):2476-96.

7. Puh, U., A. Vovk, F. Sevsek, and D. Suput. Increased cognitive load during simple and complex motor tasks in acute stage after stroke. Int J Psychophysiol. 2007;63(2):173-80.

8. Marshall, R.S., G.M. Perera, R.M. Lazar, J.W. Krakauer, R.C. Constantine, and R.L. DeLaPaz. Evolution of cortical activation during recovery from corticospinal tract infarction. Stroke. 2000;31(3):656-61.

9. Wiese, H., P. Stude, R. Sarge, K. Nebel, H.-C. Diener, and M. Keidel. Reorganization of motor execution rather than preparation in poststroke hemiparesis. Stroke. 2005;36(7):1474-9.

10. Ramoser, H., J. Muller-Gerking, and G. Pfurtscheller. Optimal spatial filtering of single trial EEG during imagined hand movement. IEEE Trans Rehabil Eng. 2000;8(4):441-6.

11. Park, C.H., W.H. Chang, S.H. Ohn, S.T. Kim, O.Y. Bang, A. Pascual-Leone, et al. Longitudinal changes of resting-state functional connectivity during motor recovery after stroke. Stroke. 2011;42(5):1357-62.

12. Rehme, A.K., S.B. Eickhoff, C. Rottschy, G.R. Fink, and C. Grefkes. Activation likelihood estimation meta-analysis of motor-related neural activity after stroke. Neuroimage. 2012;59(3):2771-82.

13. Wilke, C., L. Ding, and B. He. Estimation of time-varying connectivity patterns through the use of an adaptive directed transfer function. IEEE Trans Biomed Eng. 2008;55(11):2557-64.

14. Li, F., B. Chen, H. Li, T. Zhang, F. Wang, Y. Jiang, et al. The time-varying networks in P300: a task-evoked EEG study. IEEE Trans Neural Syst Rehab Eng. 2016;24(7):725-33.

15. Li, F., W. Peng, Y. Jiang, L. Song, Y. Liao, C. Yi, et al. The Dynamic Brain Networks of Motor Imagery: Time-Varying Causality Analysis of Scalp EEG. Int J Neural Syst. 2019;29(1):1850016.

16. Dong, L., F. Li, Q. Liu, X. Wen, Y. Lai, P. Xu, et al. MATLAB Toolboxes for Reference Electrode Standardization Technique (REST) of Scalp EEG. Front Neurosci. 2017;11:601.

17. Yao, D. A method to standardize a reference of scalp EEG recordings to a point at infinity. Physiol Meas. 2001;22(4):693.

18. Arnold, M., X. Milner, H. Witte, R. Bauer, and C. Braun. Adaptive AR modeling of nonstationary time series by means of Kalman filtering. IEEE Trans Biomed Eng. 1998;45(5):553-62.

19. Lütkepohl, H., *New introduction to multiple time series analysis*. 2005: Springer Science & Business Media.

20. Campi, M. *Performance of RLS identification algorithms with forgetting factor: A φ-mixing approach*. in *J Math Systems Estim Control*. 1994. Citeseer.

21. Rubinov, M. and O. Sporns. Complex network measures of brain connectivity: uses and interpretations. NeuroImage. 2010;52(3):1059-69.

22. Raffin, E., J. Mattout, K.T. Reilly, and P. Giraux. Disentangling motor execution

from motor imagery with the phantom limb. Brain. 2012;135(2):582-95.

23. Sharma, N. and J.-C. Baron. Does motor imagery share neural networks with executed movement: a multivariate fMRI analysis. Front Hum Neurosci. 2013;7:564.

24. Li, H., G. Huang, Q. Lin, J. Zhao, Q. Fu, L. Li, et al. EEG Changes in Time and Time-Frequency Domain During Movement Preparation and Execution in Stroke Patients. Frontiers in Neuroscience. 2020;14.

25. Li, H., G. Huang, Q. Lin, J.L. Zhao, W.A. Lo, Y.R. Mao, et al. Combining Movement-Related Cortical Potentials and Event-Related Desynchronization to Study Movement Preparation and Execution. Front Neurol. 2018;9:822.

26. Rowe, J., K. Friston, R. Frackowiak, and R. Passingham. Attention to action: specific modulation of corticocortical interactions in humans. Neuroimage. 2002;17(2):988-98.

27. Andersen, R.A. and H. Cui. Intention, action planning, and decision making in parietal-frontal circuits. Neuron. 2009;63(5):568-83.

28. Buschman, T.J. and E.K. Miller. Top-down versus bottom-up control of attention in the prefrontal and posterior parietal cortices. Science. 2007;315(5820):1860-2.

Figures

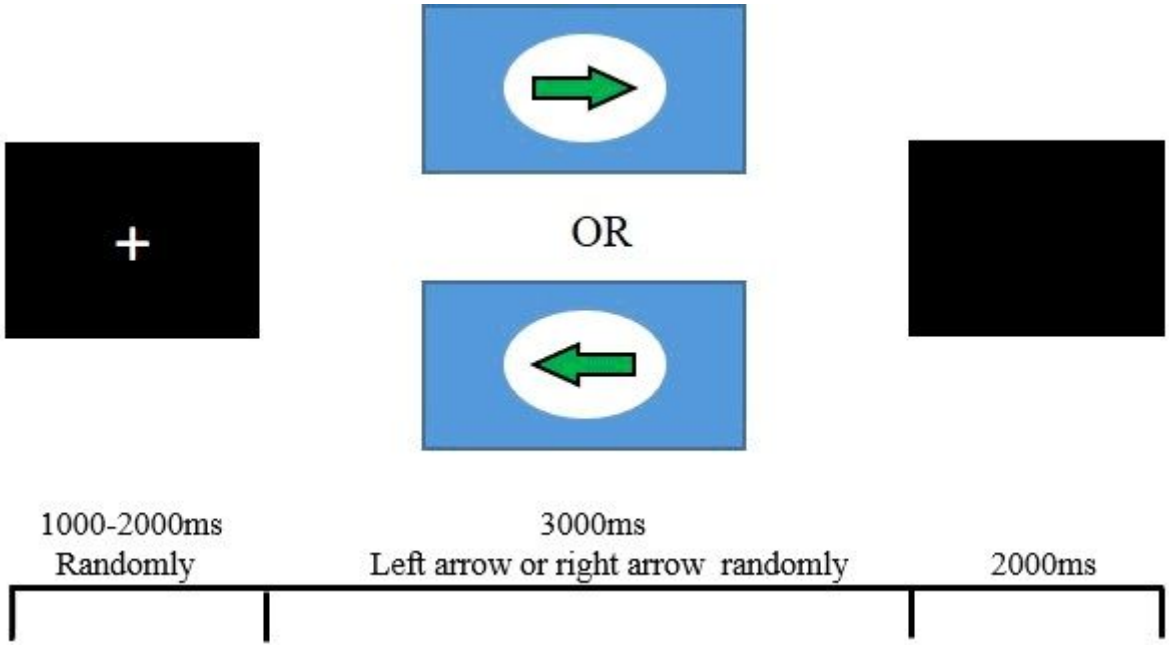

Figure 1

The experimental procedures and the timeline of a task trial.

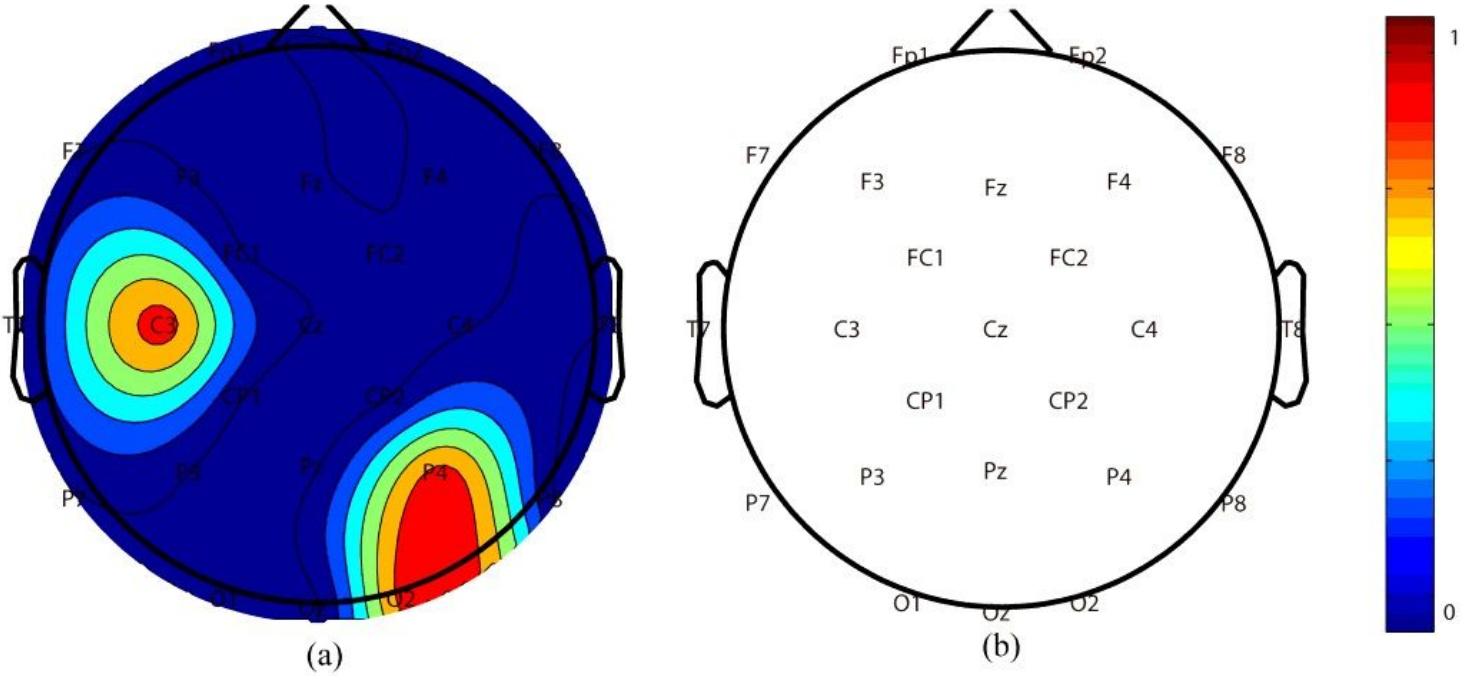

Figure 2

Scalp PSD topographies in 8 - 30 Hz. (a) Between PL and HC groups and (b) Between PR and HC groups. The regions printed with deep red color denote the PSD of the PL/PR group is significantly greater than the HC group, and the blue denotes the opposite.

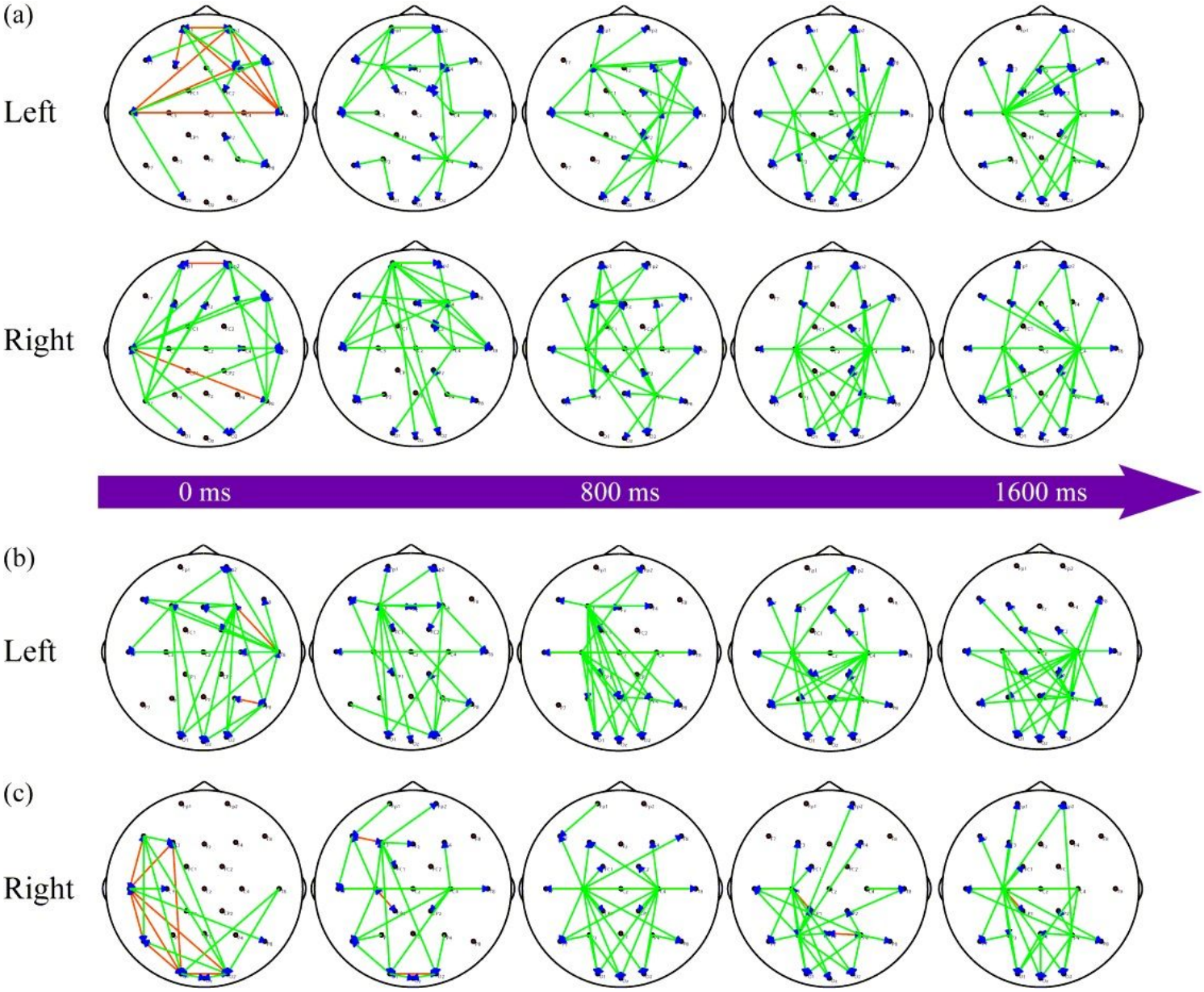

Figure 3

Time-varying information flow when achieving the wrist extension. (a) HC subjects, (b) PL subjects, and (c) PR subjects. In each subfigure, the solid green lines indicate the directed information flows, the arrows indicate the directions of information flows, and the solid red lines denote bidirectional information flows.

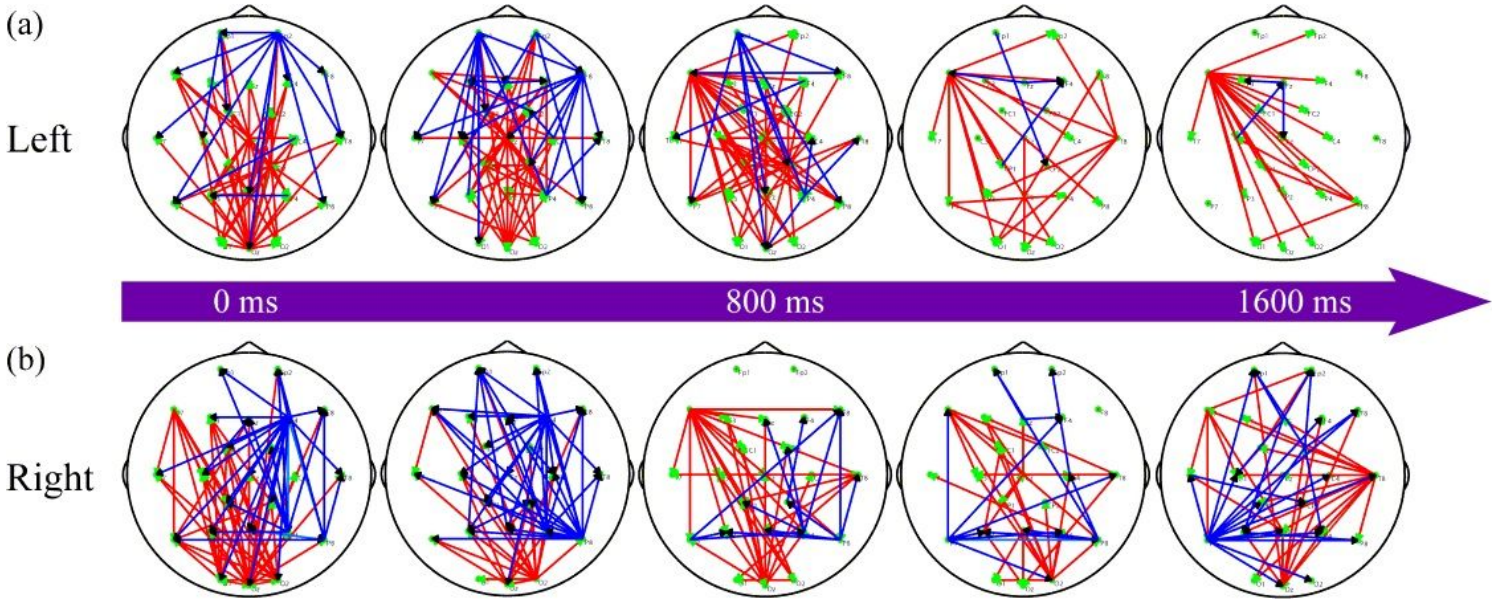

Figure 4

Differential time-varying network topologies between the pairwise groups. (a) PL versus HC groups and (b) PR versus HC groups. In each subfigure, the red and blue solid lines indicate significantly stronger and weaker directed information flows of the PL/PR group than the HC group, respectively.

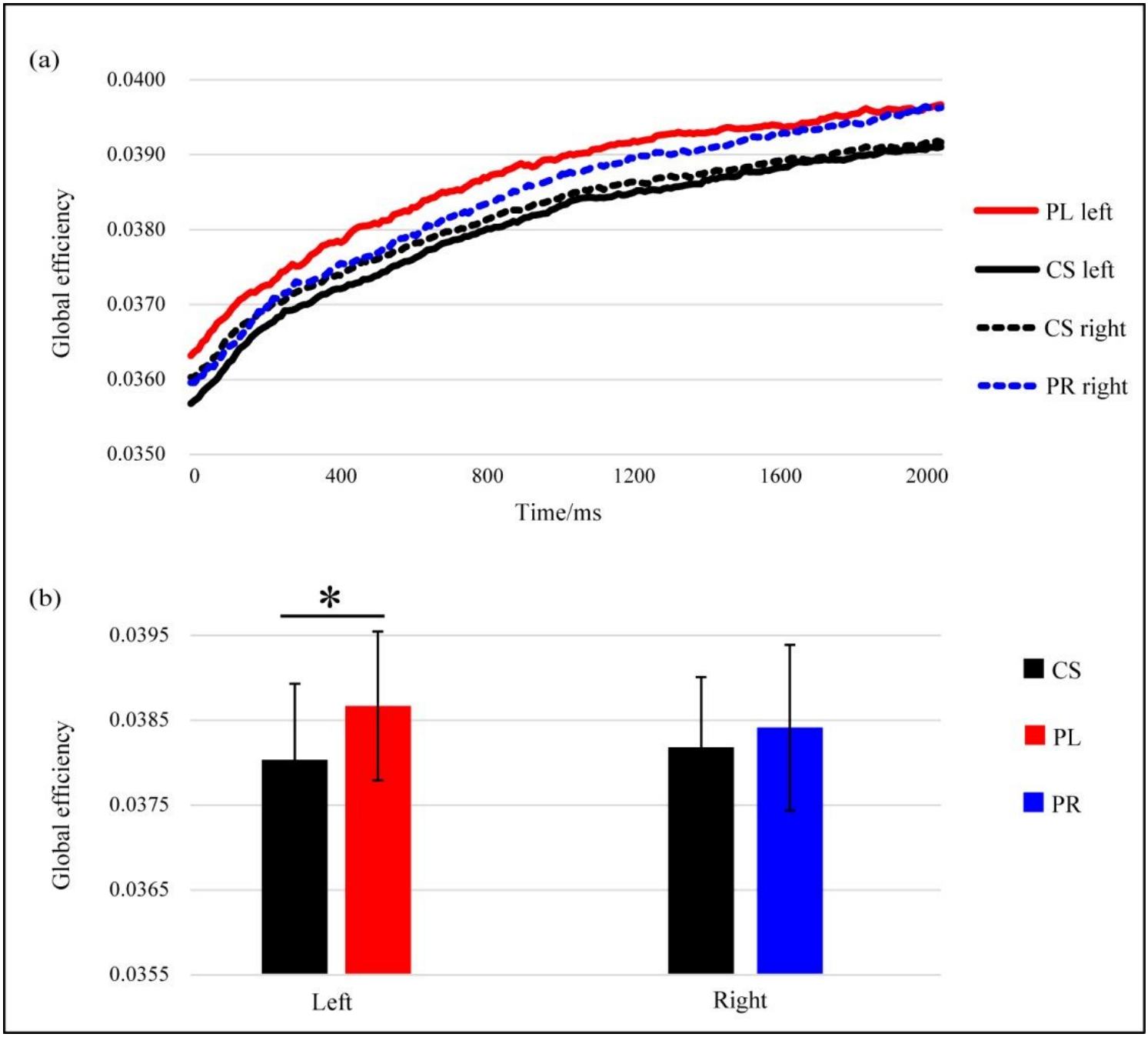

Figure 5

The time-varying GE of the three groups. (a) Dynamics of the GE and (b) Statistics of the average GE.